

## AMORPHOUS SILICON – A PROMISING MATERIAL FOR DIODES WITH ULTRA THIN ABSORBER

H. Stiebig<sup>\*</sup>, V. Mandryka<sup>a</sup>, E. Bunte, H.-J. Büchner<sup>a</sup>, K. H. Jun, G. Jäger<sup>a</sup>

Institute of Photovoltaics, Research Center Jülich, D-52425 Jülich, Germany

<sup>a</sup>Institute of Measurement and Sensor Technology, Technische Universität Ilmenau, D-98684 Ilmenau, Germany

Novel interferometers for length and displacement measurements based on sampling an optical standing wave will be presented. The interference of two laser beams propagating in opposite direction results in a sinusoidal light intensity profile, which can be detected by thin transparent photodiodes based on amorphous silicon. Two individual detectors positioned on the optical axis of a standing wave allow bi-directional fringe counting. The operation principle of set-ups consisting of two individual nip-photodiodes on one hand and a phase sensitive transparent photodiode based on two integrated nip-diodes on the other hand will be discussed. With both set-ups Lissajous figures are detected demonstrating the feasibility of the new concept for length and displacement measurements.

(Received July 3, 2003; accepted August 28, 2003)

*Keywords:* Amorphous silicon, Photodiode, Photodetector, Interferometer

### 1. Introduction

Interferometric measurements of the length or related physical values are imported in the areas where nanoscale resolution is combined with large measuring ranges which varies from a few tenth of a micrometer to meters. Typical applications are in the field of high precision measurements or positioning of objects with a nanometer accuracy which become more and more important in industrial manufacturing processes. The state-of-the-art set-up for these tasks is the Michelson interferometer. These conventional interferometers are based on the splitting of a laser beam into two part-beams and their superposition in the same propagation direction [1, 2].

As an alternative to the standard approach, two novel interferometers utilizing the interferences of waves propagating in opposite direction will be presented. For technical application as wavelength sensitive detectors [3], interferometers [4, 5] and spectrometers [6, 7], the use of the effect of a standing wave has been discussed recently, however, the fabrication of such devices has been limited by technological reasons. The detector systems based on sampling a standing wave are of high interest due to the simple set-up and the possibility to reduce the size and the number of components to a minimum. The general operation principle of a standing wave interferometer is based on the detection of the displacement of a standing wave by a transparent diode with an absorption layer thinner than the wavelength of the incident light in the material. The operation principle of interferometers based on sampling a standing wave is illustrated in Fig. 1. The standing wave is formed in front of a plane mirror due to the interference of the light beam striking orthogonally onto the plane mirror and the reflected beam. The interference pattern is characterized by the minima and maxima of the intensity. Introducing a transparent detector into the standing wave allows us to measure the intensity pattern at a specific position [8, 9] when the standing wave is not significantly affected by the detector. Varying the position of the mirror results in a phase shift of the standing wave and consequently to a change in the optical generation profile within the diode.

---

\* Corresponding author: H.Stiebig@fz-juelich.de

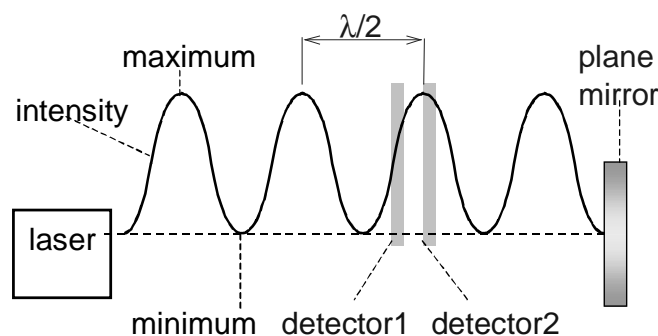


Fig. 1. Sketch of the operation principle of a standing wave interferometer.

A second detector is used for recognizing the direction of the relative movement between the mirror and the detectors [4, 10]. Thus, bi-directional fringe counting is possible. The distance between the two centers of the absorption layers of the detectors renders the optical retardation between the diodes. The phase between the photocurrents of the detectors forms elliptic Lissajous figures, when the signals are displayed on the x- and y-channel of an oscilloscope. In this kind of system, the relative displacement of the mirror and the detectors can be determined with an accuracy of  $\pm\lambda/2$ .

The performance of interferometric sensors is mainly determined by the design of the diodes due to the interaction of the standing wave and the sensor. In order to achieve a high sensor performance certain conditions have to be fulfilled: (i) high transparency of the sensor to avoid a disturbance of the standing wave pattern, (ii) high cut-off frequency, which is mainly determined by the product of the geometric capacitance of the detector and the resistance of the transparent contacts, (iii) low dark current to achieve a high dynamic and (iv) a nearly sinusoidal signal of the photocurrent with a wide difference between the maximum and the minimum photocurrent, when the detector is employed into a standing wave.

Promising materials and technologies for the fabrication of these kinds of detectors are amorphous silicon and its alloys prepared by plasma enhanced chemical vapor deposition (PECVD) at low temperature and transparent conductive oxide (TCO) prepared by sputtering. Such deposition techniques offer the possibility of a low cost production on large area and take benefit from the growing market in the area of flat panel displays and thin-film silicon solar cells. Amorphous silicon exhibits a high photosensitivity from the UVA (ultra violet A) to the near IR (infrared) part of the spectrum [11, 12]. In order to match the demand of different applications, the optical band gap as well as the transport properties of amorphous silicon based materials can be controlled over a wide spectral range by varying the deposition conditions to fabricate novel devices e.g. color sensors and sensor arrays [13].

In general, different device structures e.g. photo resistor, photo transistor or photodiode can be used as a transparent detector. For the present purpose, a n-i-p photodiode of amorphous silicon and its alloys is most advantageous, because this device structure permits the optimization of the optical and electrical properties to a certain extent independently from each other [8]. The application of n-i-p diodes with an ultra thin absorber layer ( $d_i < 50$  nm) ranges from UV-sensitive detectors up to micro interferometric sensors and sensors for spectral imaging. Such ultra-thin sensors will have also an important contribution to micro-machining applications [14].

In this paper we compare two possible set-ups which demonstrate the feasibility of our concept. For the first set-up, two individual nip-photodiodes are installed in the standing wave. Each single nip-diode, as shown in Fig. 2a, is manufactured from amorphous silicon based materials embedded between two TCO layers on a glass substrate. The TCO acts both as contact layer and anti-reflection coating. Mainly, the photo-generated carriers within the intrinsic layer of the nip-diode determine the photocurrent of the detector. The two devices installed orthogonally on the optical axis generate two signals which can be used for the displacement measurements.

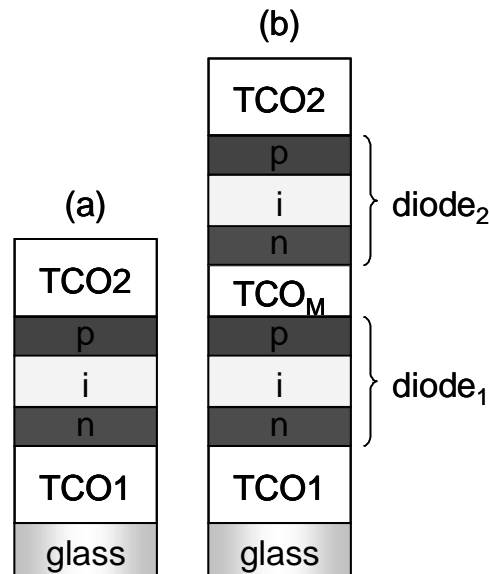


Fig. 2. Detector design of a single n-i-p diode (a) and a phase sensitive transparent detector, PSTD (b).

The second set-up presents a simpler set-up of the interferometer which can be implemented with an assembly as shown in Fig. 2b. It shows an integrated solution of two photodiodes, a so-called phase-sensitive transparent detector (PSTD). The optical retardation between the centers of the absorber layers, which determines the phase shift between the two diodes, can not be tuned after the fabrication process of PSTD is completed. However, this solution is preferable due to the simplicity of the optical set-up, which promises a reduction of cost and dimension compared to state-of-the-art interferometers.

## 2. Experiment

A  $10 \times 10 \text{ cm}^2$  Corning glass (type 1737F, 1,1 mm thickness) was used as substrate for the thin-film devices. The preparation of the TCO layers was performed by rf-magnetron sputtering of aluminium doped zinc oxide (ZnO) [15]. In order to achieve a high conductivity for TCO<sub>I</sub> the layer is prepared at 400 °C whereas TCO<sub>II</sub> and TCO<sub>M</sub> were sputtered at room temperature to prevent a damage of the amorphous layer system. The amorphous silicon and its alloy layers were deposited in a multi-chamber PECVD system at 210 °C as a n-i-p layer sequence. In order to vary the optical band gap ( $E_g$ ) of the absorber layer the layers were prepared using a gas mixture of silane, methane and hydrogen. The optical band gap increase with enhanced carbon content. The absorber layer investigated here consist of amorphous silicon (a-Si:H) and amorphous silicon carbide (a-SiC:H) and has an  $E_g$  of 1.75 eV and 2.0 eV, respectively. The p-layer was realized with a-SiC:H ( $E_g = 1.9 \text{ eV}$ ), whereas the n-layer consists of a-Si:H ( $E_g = 1.75 \text{ eV}$ ). P- and n-type doping of these layers were performed by adding trimethylboron and phosphine to the process gases, respectively [12]. Since the thickness of the amorphous layer system is below 100 nm, special efforts were attempted to avoid shunt problems, e.g. the sputtering rate for TCO<sub>II</sub> and TCO<sub>M</sub> was lowered to keep the kinetic energy of the striking particles low. More details on the sputtering and the deposition parameters can be found elsewhere [12, 15].

The detectors were patterned using photolithography and reactive ion etching. The single diode (Fig. 2a) and diode<sub>1</sub> of the PSTD (Fig. 2b) has an area of  $10.7 \text{ mm}^2$ . The area of diode<sub>2</sub> was  $8.9 \text{ mm}^2$  to enable a contacting of the underlying diode<sub>1</sub>. The photocurrent measurements within the standing wave are performed using a stabilized He-Ne laser ( $\lambda = 633 \text{ nm}$ ) with a power of 1.65 mW.

### 3. Results and discussion

#### 3.1 Optical properties of ultra-thin transparent diodes

An important criterion of a standing wave detector is its transparency, which depends on the multi-layer stack design. The detector is optimized for high transmission and low reflection at  $\lambda = 633$  nm, which is the wavelength of the He-Ne laser. Therefore, the optical thickness of the TCO<sub>I</sub>-nip-TCO<sub>II</sub> layer stack (Fig. 2a) has to be  $k_0 * \lambda_{\text{device}}/2$ . Consequently, the optical thickness of the layer stack should be equal to  $(k_1 * \lambda_{\text{TCO}}/4) : (\lambda_{\text{nip}}/2) : (k_1 * \lambda_{\text{TCO}}/4)$  with  $k_0, k_1 = 1, 2, 3, \dots$ . Fig. 3 exhibits simulated reflection spectra from standing wave detectors with different TCO layer thicknesses. The simulations were carried out for  $1 \leq k_1 \leq 5$ . Using the optical refractive index of the TCO at  $\lambda = 633$  nm leads to a TCO layer thickness of around  $k_1 * 83$  nm. Only for  $k_1 = 1$  the reflection (R) shows a broad minimum between 550 and 750 nm. With increasing  $k_1$  the region, where the minimum in R is observed, shrinks and consequently, the device becomes more sensitive to small thickness variations. If the TCO layer is used as an anti-reflection coating (odd  $k_1$  values) the reflection of the device is significantly reduced in the vicinity of the minimum compared to simulations with even  $k_1$  values. Particularly for even  $k_1$  values, a small mismatch of the TCO layer thickness results in a shift of the minimum of the reflection and a sharp increase of the reflection at 633 nm. The deviation of the layer thickness from the ideal value can be caused by variations of the deposition conditions. The simulated curves are in good agreement with the measured data (not shown), when a measuring set-up with a light source (e.g. halogen lamp) with a coherence length in the micrometer range is used. Similar conditions are also given if the spectral sensitivity of the device is measured using a differential spectral response (DSR)-measurement set-up. However, applying a light source with a long coherence length results in relatively short wavelength oscillations in the reflectance spectra as calculated in Fig. 4. The figure shows the simulated reflectance of a transparent detector based on a  $(3 * \lambda_{\text{TCO}}/4) : (\lambda_{\text{nip}}/2) : (3 * \lambda_{\text{TCO}}/4)$  layer stack taking into account coherent and incoherent wave propagation through the glass substrate with a thickness of 1.1 mm [17, 18]. These oscillations can be experimentally observed when a light source is applied with a coherence length longer than twice the thickness of the glass substrate. A light source with a coherence length between several meters and kilometers is the He-Ne laser [16]. Thus, Fig. 4 implies that a certain difference between the characteristics of R, T and DSR and the real performance of the device (detector within the standing wave) can come from the different coherent length of the light source due to interferences within the glass substrate.

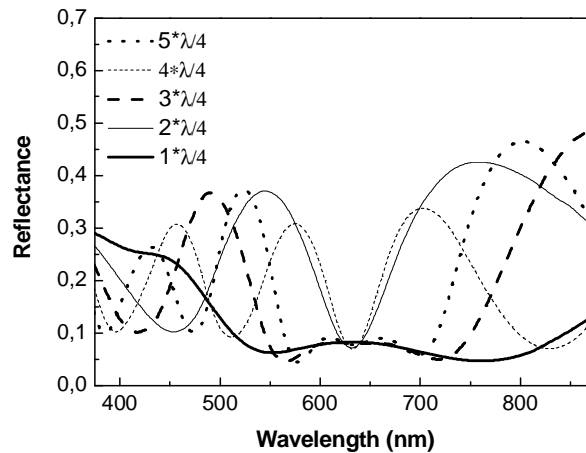


Fig. 3. Calculated reflectance of a multi-layer stack glass-TCO<sub>I</sub>:nip:TCO<sub>II</sub>. The optical thickness of the thin film system is  $(k_1 * \lambda_{\text{TCO}}/4) : (\lambda_{\text{nip}}/2) : (k_1 * \lambda_{\text{TCO}}/4)$ .  $k_1$  was varied from 1 to 5. For the simulations only incoherent wave propagation was considered within the glass substrate.

The thickness of the transparent conductive layers has also a significant influence on the electrical behavior of the detector. The conductivity of the aluminium doped ZnO and consequently the cut-off frequency of the device improves with increasing layer thickness. Particularly, the impact of the nucleation region of the ZnO layers limits the conductivity of thin layers [19]. Consequently, the optimized design concept consists of a n-i-p diode with a thickness of  $\lambda_{\text{nip}}/2$  and a TCO front and back contact with an optical thickness of around  $3\lambda_{\text{TCO}}/4$ .

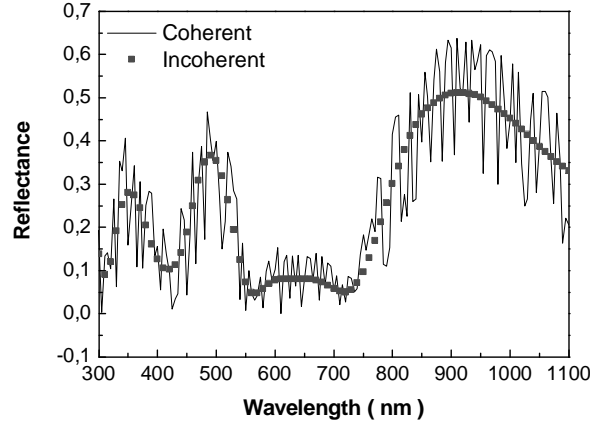


Fig. 4. Calculated reflectance of a stack glass-TCO<sub>i</sub>nip: TCO<sub>II</sub>. The thickness of the system is  $(3*\lambda_{\text{TCO}}/4):(\lambda_{\text{nip}}/2):(3*\lambda_{\text{TCO}}/4)$  and coherent and incoherent wave propagation within the glass substrate were taken into account.

### 3.2 Optoelectronic properties of ultra-thin transparent diodes

The design of the n-i-p diode is investigated in more detail to determine the optimal i-layer thickness. A standing wave can be described by the superposition of two waves propagating in opposite directions. The spatial intensity distribution within the i-layer of the diode can be described as follows:

$$I_i(x) = I_0 T_i(\lambda) \left( e^{-\alpha_i x} + (\tau_2)^2 \cdot e^{-\alpha_i(2d_i-x)} - 2\tau_2 \cdot e^{-\alpha_i d_i} \cdot \cos\left(\frac{4\pi}{\lambda} n_i(d_i-x) + 2\xi_2\right) \right) \quad (1)$$

$I_0$  is the incident light intensity,  $T_i(\lambda)$  corresponds to an internal transmission of the detector up to the i-layer, and  $\alpha_i$  is the absorption coefficient of the i-layer.  $\tau_2$  and  $\xi_2$  are the amplitude and the phase of the transmittance of the layer system behind the i-layer. The first term  $e^{-\alpha_i x}$  of Eq. (1) originates from the electric field propagation into positive direction. The positive direction means the direction of the incident light. The second term  $e^{-\alpha_i(2d_i-x)}$  describes the electric field propagation into negative direction. The third term is due to interference effects of the two waves. Assuming a sufficiently low absorption, no reflectance of the detector, and an ideal plane mirror the intensity distribution within the i-layer ( $I_i(x)$ ) is given by:

$$I_i(x) = I_0 \left( 2 - 2\cos\left(\frac{4\pi}{\lambda} n_i \cdot x\right) \right) \quad (2)$$

The intensity varies between 0 and  $4I_0$ . For detectors with an infinitely thin absorber layer the interference pattern according to Eq. (2) can be recorded. However, the optoelectronic properties of an amorphous diode without an i-layer shows a low photosensitivity and a high dark current [20]. To estimate the influence of the i-layer thickness on the device performance we have calculated the

expected photocurrent as a function of the i-layer thickness by the use of Eq. (2). For these calculations we have considered that the photo-generated carriers within the i-layer dominantly contribute to the photocurrent. The photocurrent is nearly proportional to the integration of the spatial intensity distribution within the i-layer. Fig. 5 shows the calculated photocurrents as a function of the normalized absorber layer thickness when the center of the i-layer is located at a maximum or at a minimum of a standing wave. An absorber layer positioned at an intensity minimum or maximum results in a minimal photocurrent  $i_{\min}$  or maximal photocurrent  $i_{\max}$ , respectively. As plotted in Fig. 5, both extremal values increase with increasing i-layer thickness. The difference between the extremal values, indicated by the arrows, will lead to the amplitude of the alternating component  $i_{\sim}$  of the photocurrent when the mirror is moved. Thus, the measured photocurrent  $i_{\text{ph}}$  can be considered as a superposition of an alternating component  $i_{\sim}$  and a direct component  $i_{\sim}$  (Eq. (3)).

$$i_{\text{ph}} = i_{\sim} + i_{\sim} \quad (3)$$

The direct component  $i_{\sim}$  increases linearly with the absorber layer thickness. To achieve a high difference between the minimum and maximum value of the photocurrent, the amplitude of the alternating component  $i_{\sim}$  should be maximized. Fig. 5 shows that this condition is satisfied at i-layer thicknesses of  $d_i = \lambda_i/4n$  and  $3\lambda_i/4$ . To minimize absorption losses within the detector, an i-layer thickness close to  $d_i = \lambda_i/4$  was chosen for the fabricated diodes. It is worth to note that, for  $d_i = \lambda_i/2$  and  $d_i = \lambda_i$  the amplitude of the alternating component  $i_{\sim}$  is 0, since  $I_{\max}$  equals  $I_{\min}$ . In this case, the thickness of the i-layer ( $d_i = \lambda_i/2$  or  $d_i = \lambda_i$ ) fits exactly with one or two intensity periods of the laser beam and consequently, no movement of the mirror can be detected.

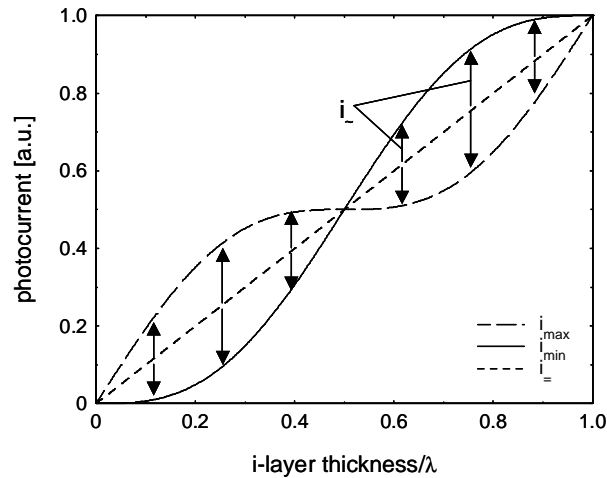


Fig. 5. Calculated photocurrent of a single nip-diode as a function of the normalised absorber layer thickness.

To quantify the ability to distinguish between the maximum and minimum as a function of the i-layer thickness, which coincides with the amplitude of the alternating component of the photocurrent, the standardized difference (SD) is widely used. The SD is defined as the quotient of  $i_{\sim}$  and the measured current in the absence of the mirror. In the latter case, the laser beam penetrates the diode only once. Thus, the current measured without using a mirror is similar to half of  $i_{\sim}$ . In agreement with the discussion of Fig. 5, SD is zero for an i-layer thickness  $d_i = \lambda_i/2$  and  $d_i = \lambda_i$ . Considering the different optical refractive indices of a-Si:H and a-SiC:H the minimum in SD at  $d_i = \lambda_i/2$  correlates with an i-layer thickness of around 80 and 90 nm, respectively. As a compromise between the requirements regarding a high SD and a low geometric capacitance,  $C_{\text{geo}} \sim 1/d_i$ , we chose an i-layer thickness of around 30-40 nm, at which a SD between 2 and 3 can be theoretically achieved (see Fig. 6).

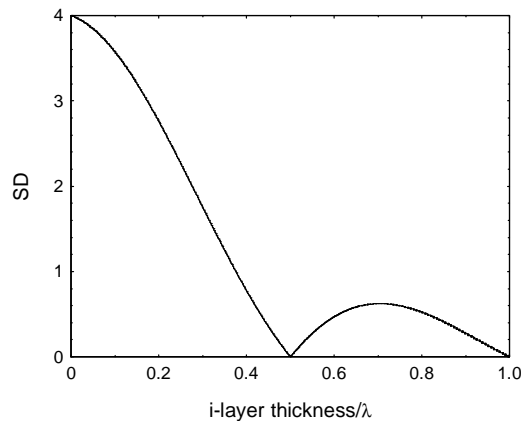


Fig. 6. Calculated standardized difference (SD) as a function of the i-layer thickness. The SD is defined as the quotient of the difference between the maximum and minimum of the photocurrent and the measured current in the absence of the plane mirror.

Besides the thickness of the i-layer also its absorption properties has an influence on the device performance (see Eq. (1)). Fig. 7 depicts the effect of three different absorber designs on the optoelectronic behaviors of the diode. For diode structure A, the i-layer consists of an entirely a-Si:H layer with a band gap ( $E_g$ ) of around 1.75 eV. In structure B, an a-SiC:H layer ( $E_g = 2$  eV) is employed. The absorber layer of structure C is separated into two regions of similar thickness of around 15-20 nm. The a-SiC:H layer is arranged next to the p-layer. The dark I/V-characteristics of the realized diodes are plotted in Fig. 7. Due to the lower band gap (higher intrinsic carrier density) of a-Si:H compared to a-SiC:H, the dark I/V curve of the corresponding diode is nearly parallelly shifted to higher values. Structure C behaves similar to structure B, because at higher voltages ( $0.6\text{V} < V < 1\text{V}$ ) the transport and recombination of carriers within the wide band gap material mainly determines the I/V characteristics [20, 21].

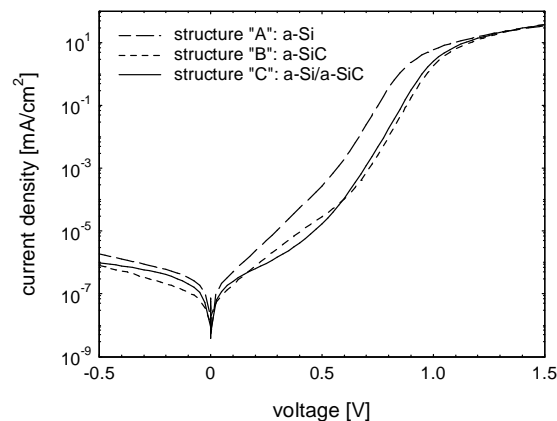


Fig. 7. Dark I/V curves of n-i-p diodes with different absorber material in the i-layer.

Although the total diode thickness is only between 80 nm and 90 nm and the i-layer is only around 30-40 nm the current density is very low ( $I_{\text{dark}} < 2 \times 10^{-6}$  mA/cm<sup>2</sup>) in the bias range  $-0.5\text{V} < V < 0\text{V}$ . Since the diode operates in this bias range a high dynamic range is achieved. For  $V > 0.8\text{V}$  the I/V curves deviate from the nearly linear behavior using a log-scale for the current density. The saturation of the current density is mainly attributed to the resistance of the TCO layers. This resistance dominates in combination with  $C_{\text{geo}}$  the RC-constant of the device and consequently the cut-off frequency of the detector. Although neither the design of the multi layer stack, the

adjustment of the size of the detector on the spot of the laser beam, nor the contact design is optimized yet, a cut-off frequency of up to 200 kHz was achieved for such kind of diodes.

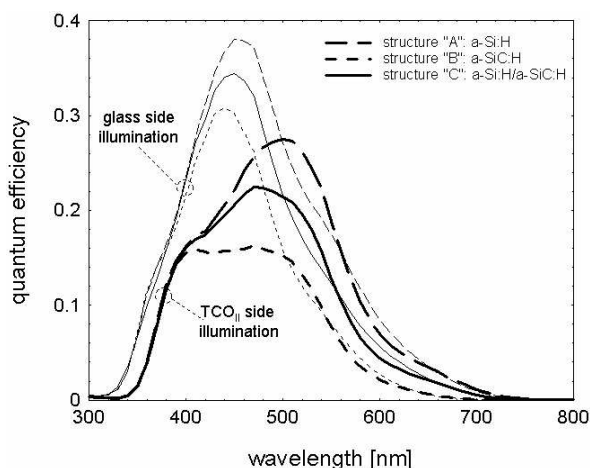


Fig. 8. Quantum efficiency curves of n-i-p diodes with different absorber material in the i-layer. The transparent detectors are characterized from both sides.

The spectral sensitivity of the three diodes measured under short circuit conditions and illuminated from both sides is shown in Fig. 8. Since the p-layer is thicker ( $>30$  nm) than the n-layer (20 nm) the rising edge of the quantum efficiency is shifted to shorter wavelengths when the light penetrates through the glass side. In the long wavelength range and under both sides of illumination the quantum efficiency QE of structure A is higher than for structure B, according to the different absorption coefficient of a-Si:H and a-SiC:H. The low absorption of structure B leads to a transmittance at 633 nm exceeding 85%. The QE of structure C is in between the QE of structure A and structure B, because the absorption region of structure C contains both materials to equal dimensions. The main advantage of structure B is the high yield of detectors with a good device performance (low dark current and no shunt problems) above 90%. The yield for structure C and A is around 80% and 30%, respectively. This result can be explained by the different microstructure of a-Si:H and a-SiC:H [22]. Since the fabrication of structure B is simpler as structure C, we have focused our investigations on diodes with a design according to structure B.

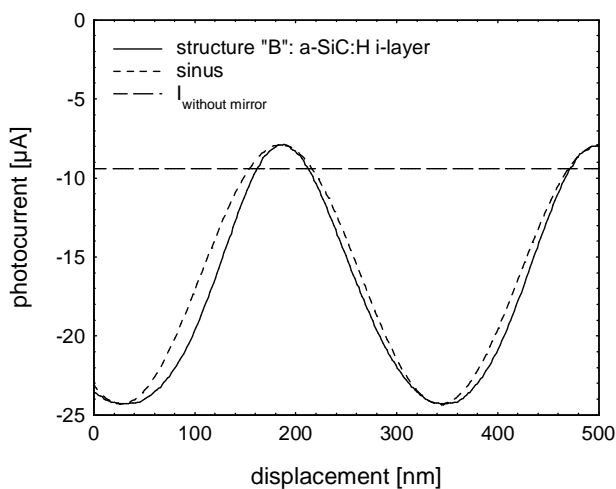


Fig. 9. Measured photocurrent of the detector with an entirely a-SiC:H absorber (structure B) while the plane mirror is moved. Additionally, a sinus - function and the measured photocurrent without using a mirror is plotted.

The transparent diode (structure B) is introduced into a standing wave and the plane mirror is moved. The interference signal of the transparent photodetector shows a nearly sinusoidal dependency on the displacement with a period corresponding to half of the wavelength of the laser beam (Fig. 9). Additionally, a sinus-function and the measured photocurrent without using a plane mirror are plotted. For structure B a SD of 1.78 is evaluated. SD of the three diodes varies between 1.2 and 2 and SD of structure B is higher than SD of structure A due to the lower absorption within the i-layer. However, these values are lower than predicted by the calculations (Fig. 6). Under ideal conditions, the deviation in SD from the expected value between 2 and 3 can be used to estimate an upper limit for the implemented i-layer thickness. Considering a value of 1.78 and using Fig. 6 implies an i-layer thickness of around 40 nm, which is slightly higher than the expected value estimated by the deposition rate of single layers. The deviation of the layer thickness is still within the technological tolerance. This result indicates that the “real” thickness of the i-layer was slightly underestimated. The whole layer thickness was measured by mechanical thickness measurements to control the deposition conditions. Further reasons which lead also to a deviation of the measured signal from the sinus-function as well as a lower SD are (i) absorption and reflection losses (see Eq. (1)), (ii) collection of carriers generated in the doped layers and (iii) multiple reflection of the light within the detector mainly caused by small thickness deviations of the ideal thickness values ( $\lambda_{\text{nip}}/2$  and  $3\lambda_{\text{TCO}}/4$ ). Multiple reflection of the light within the layer stack results in a superposition of waves propagating in the same and opposite direction.

### 3.2 Interferometer based on two individual ultra-thin n-i-p-diodes

Introducing two individual photodiodes based on diode structure B into a standing wave allows to measure two independent photocurrents. Displaying the two currents on the x- and y-channel of an oscilloscope leads to Lissajous figures when the mirror is moved. The direction of the travel clockwise or anti clockwise on the screen depends on the direction of the movement of the mirror. A phase  $\gamma$  of  $\gamma \neq 0^\circ, 180^\circ, \dots$ , between these two signals allows bi-directional fringe counting. If the phase shift is  $\gamma = 0^\circ, 180^\circ, \dots$ , the ellipse shrinks to a single line and the determination of the direction of the displacement is not possible. By tuning the distance between the single photodetectors, which is defined by the different spatial arrangement of the centers of the i-layer within the standing wave, to  $90^\circ$ , the Lissajous figure fits with a perfect circle. For this ideal case, an accuracy in the nm-range can be achieved by subdivision of the Lissajous figure, since the two signals form an orthogonal system. Fig. 10 shows as an example two elliptic Lissajous figures with a phase shift between the two photocurrents close to  $90^\circ$  (Fig. 10, left side) and of around  $50^\circ$  (Fig. 10, right side). For this purpose one diode was mounted on a piezo actuator, which allows an adjustment of  $\gamma$  over the entire range from  $0^\circ$  to  $360^\circ$ . For data processing only the alternating component of the photocurrent has been considered and the unit of the signal is given in voltage, since current-voltage amplifiers were used.

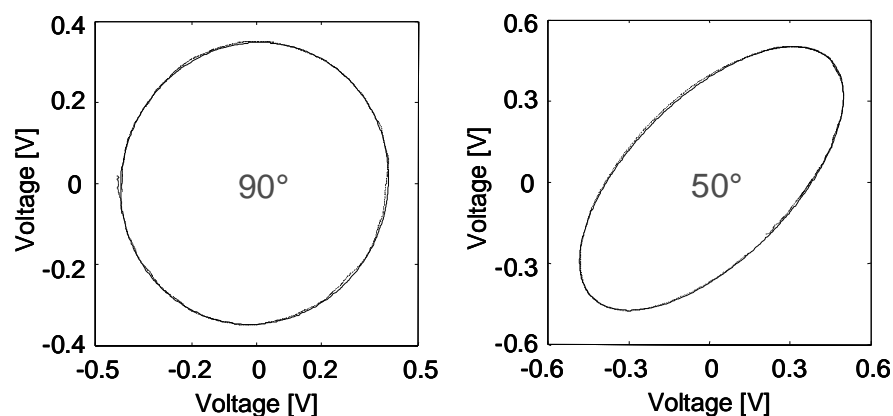


Fig. 10. Lissajous figures obtained by a xy-display of the photocurrent of two individual diodes with different relative positions of the diodes on the optical axis of the standing-wave pattern.

### 3.3 Phase sensitive transparent detector (PSTD)

A reduction of the components of the mechanical set-up can be achieved by the integration of the individual diodes (see Fig. 2b). In the following, the influence of the device design of the PSTD on the properties of the interferometer will be discussed. As discussed in section 3.1, the layer stack has to be highly transmissive and low reflective at the laser wavelength of 633 nm, to avoid disturbance of the standing wave. These requirements can be fulfilled by the design rules as presented above. For a maximal transmission the optical thickness of the whole device should be equal to  $k_0 \cdot \lambda_{\text{device}}/2$  and the optical thickness of the  $\text{TCO}_I:\text{nip}:\text{TCO}_M:\text{nip}:\text{TCO}_{II}$  layer stack has to be  $(3 \cdot \lambda_{\text{TCO}}/4):(\lambda_{\text{nip}}/2):(k_2 \cdot \lambda_{\text{TCO}}/2):(\lambda_{\text{nip}}/2):(3 \cdot \lambda_{\text{TCO}}/4)$ , with  $k_2 = 1, 2, 3, \dots$ .  $\text{TCO}_M$  is embedded between the two diodes and is used as a common contact. In order to optimize the transparency of the system  $k_3$  was chosen to 1. Based on optical calculations a transmittance of around 80% is expected for the whole system. However, deviations from the idealities in the layer thickness lead to a lower measured transmission at 633 nm of about 70%.

Although the assembly consists of two very thin diodes (the structure of each diode is similar to the design of structure B), which are patterned by a two mask process, the dark current density of the individual diodes is very low ( $I_{\text{dark}} < 2 \cdot 10^{-6}$  mA/cm<sup>2</sup>) at reverse bias (not shown). The IV-characteristics fit well with the dark current of single diodes (Fig. 7). Only at high positive bias the current of the individual nip-diodes of the PSTD saturates at a lower level in comparison with single deposited diodes (Fig. 7), due to a higher series resistance of the PSTD. This can be mainly explained by the thickness of the common contact ( $\text{TCO}_M$ ) which is 2/3 of the thickness of  $\text{TCO}_I$  or  $\text{TCO}_{II}$ .

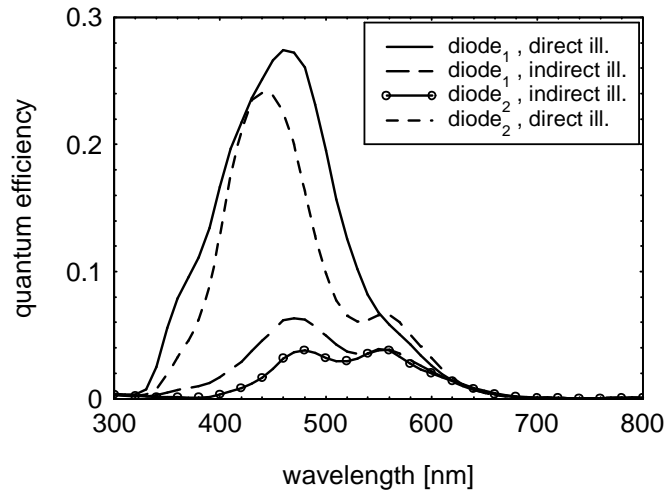


Fig. 11. Quantum efficiencies of the PSTD, illuminated from both sides.

Fig. 11 shows the spectral sensitivity of both diodes measured from either sides. The QE measured under “direct” illumination conditions (illumination from the side nearest to the diode under test) is higher than the QE at “indirect” illumination conditions (illumination from the side, where the other diode is in front of the diode under test). The lower QE under indirect illumination is due to absorption “losses” in the diode, which is in-between the side of incidence of the light and the diode under test. In this case the diode which is arranged in front of the other acts as a transmission filter. Because of the wavelength dependent absorption coefficient, absorption losses are more pronounced at shorter wavelengths. For  $\lambda > 600$  nm similar QEs are measured, which are nearly independent on the direction of illumination. The QE of both diodes at 633 nm amounts to about 1.4%.

In agreement with the discussion of Fig. 8, the rising edge of the QE of diode<sub>2</sub> is shifted to longer wavelengths compared with diode<sub>1</sub> under direct illumination, caused by the thinner n-layer thickness in comparison with the p-layer thickness. However, under indirect illumination this explanation is not applicable, because in comparison with diode<sub>2</sub> a lower blue response of diode<sub>1</sub>

should be expected. The high blue response of diode<sub>1</sub> under indirect illumination conditions is likely attributed to a measuring error since the underlying diode<sub>1</sub> has a larger area as diode<sub>2</sub> and the area of measuring spot of the spectral response set-up has a similar size as the area of diode<sub>2</sub>. Thus a small amount of light can strike directly on the larger area of the underlying diode<sub>1</sub> and it is not absorbed by diode<sub>2</sub>.

Next, the PSTD is characterized when it is implemented in the standing wave and the plane mirror is moved. A xy-plot of the photocurrent of the two diodes is given in Fig. 12 as a Lissajous figure. The photocurrent of both diodes vary between 5 and 20-25  $\mu\text{A}$ , which is within the expected range when using a laser power of 1.65 mW and considering the QE as measured in Fig. 11. The shift of the center of the ellipse out from the zero point of the coordination system can be attributed to the direct component ( $i_{\perp}$ ). The sign of measured current is a result of the measurement set-up. The TCO<sub>M</sub> contact is used as a common ground.

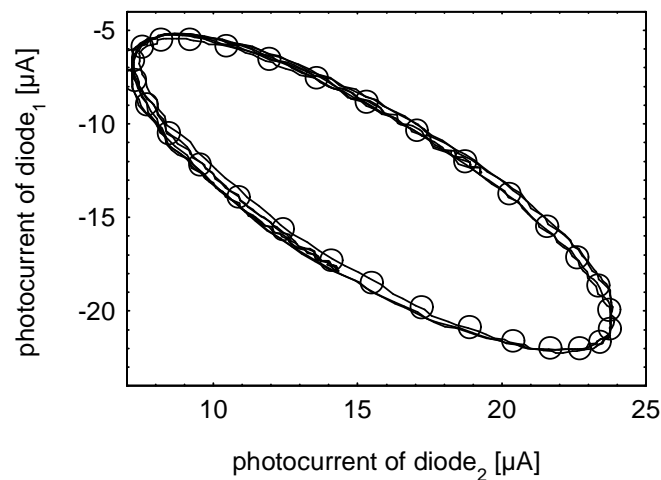


Fig. 12. Photocurrents of a PSTD measured inside the standing wave when moving the mirror. The measuring (lines) and calculated (symbols) data are displayed as a Lissajous figure.

$\gamma$  of the two currents is about  $35^\circ$ . It is determined by the optical thickness of half of the i-layer of diode<sub>1</sub>, p-layer of diode<sub>1</sub>, TCO<sub>M</sub> layer, n-layer of diode<sub>2</sub> and half of the i-layer of diode<sub>2</sub>. For high transmission the optical thickness of both n-i-p diodes and of the TCO<sub>II</sub> layer should be close to  $\lambda_{\text{device}}/2$ . However, under these conditions the phase shift between the two photocurrents would be  $360^\circ$  and the shape of the ellipse shrinks to a single line. As a consequence, the direction of the displacement of the mirror cannot be evaluated. As one approach, the thickness of the p-layer of diode<sub>1</sub> was enlarged to around 50 nm to achieve a  $\gamma$  between the two photocurrents different from  $360^\circ$ . The p-layer thickness was modified to keep the absorption losses within the doped layer at a minimum, because the band gap of the p-layer is higher than that of the n-layer. The increase in the p-layer thickness of diode<sub>1</sub> by around 10 nm is reflected in the measured phase shift (Fig. 12). It should be mentioned that a specific optimization of the layer stack in the nm-range is critical. The variations of the deposition parameters lead to thickness variations of the a-Si:H based layers, which are in the same order. The shape of the ellipse is in good agreement with the calculated ellipse (symbols) using two sine functions with the same amplitude and a phase shift of  $35^\circ$ . This result indicates that the measured current of the two diodes is also nearly sinusoidal and that the introduction of the sensor does not significantly disturb the standing wave. By interpolation of the measured ellipse using the Heydemann algorithm [23], displacement or length measurements can be determined with an accuracy of  $\pm 15$  nm [18]. To obtain a higher accuracy the thicknesses of the two i-layers, the p-layer of diode<sub>1</sub> and n-layer of diode<sub>2</sub> have to be adjusted to obtain  $\gamma$  of the photocurrents of  $90^\circ$ . A challenge for the forthcoming works will be the optimization of the PSTD with respect to an improved optical

adjustment of the whole layer stack, better tuning of  $\gamma$  between the two photocurrents and an increase of the cut-off frequency.

#### 4. Conclusions

A new concept for precision length measurement based on sampling an optical standing wave was presented. Making use of the standard thin-film technologies on glass substrate – PECVD for amorphous silicon and sputtering for TCO layers – we have developed thin transparent nip-photodiodes, which enable the detection of the standing wave. Thin photodiodes with an optically adjusted layer stack with an optical thickness close to  $(3\lambda_{\text{TCO}}/4):(\lambda_{\text{nip}}/2):(3\lambda_{\text{TCO}}/4)$  and an around 30-40 nm thick i-layer of a-SiC:H were realized with a transmittance at 633 nm above 85%. The measured interference signal of the transparent photodetector shows a nearly sinusoidal signal with a period corresponding to half of the wavelength of the He-Ne laser. Introducing two transparent photodetectors into a standing wave leads to the development of a new type of interferometer. The simplicity of the PSTD recommends this new concept for length and displacement measurements. With the fabricated detector system measurements with an accuracy of  $\pm 15$  nm can be performed.

#### Acknowledgements

The authors like to thank D. Knipp, M. Krause, T. Brammer, O. Kluth and G. Schöpe for many helpful discussions. The authors gratefully acknowledge the financial support from the “Deutsche Forschungsgemeinschaft” (JA 779/4, Sti 181/1-1).

#### References

- [1] H.-J. Büchner, G. Jäger, *Technique Measurement* **6**, 146 (1988).
- [2] M. J. Downs, W. R. C. Rowley, *Precision Engineering* **15**, 281 (1993).
- [3] D. A. B. Miller, *IEEE J. of quantum electronics* **30**, 732 (1999).
- [4] H. Büchner, *Deutsches Patent DE 33 00*, 369 (1983).
- [5] M. Minoru Sasaki, X. Mi, K. Hane, *Appl. Phys. Lett.* **75**, 2008 (1999).
- [6] H. L. Kung, S. R. Bhalotra, J. D. Mansell, D. A. B. Miller, J. S. Harris, *IEEE Journal on Selected Topics in Quantum Electronics*, **8** (1), 98 (2002).
- [7] D. Knipp, H. Stiebig, H.-J. Büchner, G. Jäger, M. Rosa, R. A. Street, Fall meeting, Mat. Res. Soc., Boston, USA, 26.-30. Nov. 2001, in print.
- [8] H. Stiebig, H.-J. Büchner, E. Bunte, V. Mandryka, D. Knipp, G. Jäger, *Thin Solid Films*, **427**, 152 (2003).
- [9] H.-J. Büchner, H. Stiebig, V. Mandryka, E. Bunte, G. Jäger, *Meas. Sci. Technol.* **14**, 311 (2003).
- [10] H. Stiebig, H. Büchner, E. Bunte, V. Mandryka, D. Knipp, G. Jäger, *Applied Physics Letters*, in press, 2003.
- [11] R. A. Street, *Hydrogenated Amorphous Silicon*, Cambridge University, Cambridge, UK, 1991.
- [12] W. Luft, Y. Tuso, *Hydrogenated amorphous silicon alloy deposition processes*, Marcel Dekker, Inc., 1993.
- [13] H. Stiebig, D. Knipp, *Physics and Applications of Disordered Materials*, editor: M. Popescu, INOE, 323 (2002).
- [14] O. Kluth, A. Löffl. S. Wieder, C. Beneking, L. Houben, B. Rech, H. Wagner, S. Waser, J. A. Selvan, H. Keppner, *Proc. 26th IEEE PVSEC*, 715 (1997).
- [15] H. L. Kung, S. R. Bhalotra, J. D. Mansell, D. A. B. Miller, 2000 IEEE/LEOS International Conference on Optical MEMS.
- [16] E. Hering, R. Martin, M. Stohrer, “*Physik für Ingenieure*” Springer Verlag Berlin Heidelberg New York (ISBN 3-540-6244-2).
- [17] H. Stiebig, A. Kreisel, K. Winz, M. Meer, N. Schultz, Th. Eickhoff, H. Wagner, *Proc. First World Conf. On Photovoltaic Energy Conversion (WCPEC)*, 603 (1994).

- 
- [18] H.-J. Büchner, E. Bunte, V. Mandryka, H. Stiebig, G. Jäger, Proc. SPIE conference „Optical Metrology“ 23-26 June, 2003, München, Germany
- [19] O. Kluth, B. Rech, H. Wagner, 17<sup>th</sup> European Photovoltaik Solar Energy Conference, Munich, Germany, 22-26. Oct. 2001.
- [20] M. Krause, M. Topic, H. Stiebig, H. Wagner, *phy. stat. sol. (a)* **185** (1), 121 (2001).
- [21] H. Stiebig, J. Zimmer, F. Siebke, J. Fölsch, H. Wagner, Proc. 14th EPVSEC, Barcelona, Spain, 554 (1997).
- [22] W. Beyer, H. Mell, in: *Disordered Semiconductors*, Plenum, New York 641, (1987).
- [23] P. L. M. Heydemann, *Appl. Opt.* **20**, 3382 (1981).